Assessment of induced SAR in children exposed to electromagnetic plane waves between 10 MHz and 5.6 GHz

2010 Phys. Med. Biol. 55 3115

(http://iopscience.iop.org/0031-9155/55/11/009)

Phys. Med. Biol. **55** (2010) 3115–3130 doi:10.1088/0031-9155/55/11/009

Assessment of induced SAR in children exposed to electromagnetic plane waves between 10 MHz and 5.6 GHz

J F Bakker[1], M M Paulides[1], A Christ[2], N Kuster[2] and G C van Rhoon[1]

[1] Erasmus MC-Daniel den Hoed Cancer Center, Department of Radiation Oncology, Section Hyperthermia, PO box 5201, NL-3008 AE, Rotterdam, The Netherlands
[2] Foundation for Research on Information Technologies in Society (IT'IS), Switzerland

E-mail: j.bakker@erasmusmc.nl

Received 25 January 2010, in final form 7 April 2010
Published 12 May 2010
Online at stacks.iop.org/PMB/55/3115

Abstract

To avoid potentially adverse health effects of electromagnetic fields (EMF), the International Commission on Non-Ionizing Radiation Protection (ICNIRP) has defined EMF reference levels from the basic restrictions on the induced whole-body-averaged specific absorption rate (SAR_{wb}) and the peak 10 g spatial-averaged SAR (SAR_{10g}). The objective of this study is to assess if the SAR in children remains below the basic restrictions upon exposure at the reference levels. Finite difference time domain (FDTD) modeling was used to calculate the SAR in six children and two adults when exposed to all 12 orthogonal plane wave configurations. A sensitivity study showed an expanded uncertainty of 53% (SAR_{wb}) and 58% (SAR_{10g}) due to variations in simulation settings and tissue properties. In this study, we found that the basic restriction on the SAR_{wb} is occasionally exceeded for children, up to a maximum of 45% in small children. The maximum SAR_{10g} values, usually found at body protrusions, remain under the limit for all scenarios studied. Our results are in good agreement with the literature, suggesting that the recommended ICNIRP reference levels may need fine tuning.

(Some figures in this article are in colour only in the electronic version)

1. Introduction

Due to the exponential increase in wireless applications, public concern over their potentially adverse health effects has also increased. In the past, safety guidelines have been developed to restrict exposure to electromagnetic fields (EMF). For the radio frequency (RF) range of 100 kHz–300 GHz, these guidelines are based on keeping the body temperature rise under 1 °C, which has been correlated to a maximum whole-body-averaged specific absorption

Table 1. ICNIRP general public reference levels for the plane wave power density S_{eq}.

f	S_{eq} (Wm^{-2})
10–400 MHz	2
400–2000 MHz	f (MHz)/200
2–300 GHz	10

rate (SAR_{wb}) of 4 W kg^{-1} for 30 min in adults (WHO 1993). To account for sensitive subpopulations such as children and the elderly, this threshold is reduced to 0.08 W kg^{-1} for the general public. While SAR limits are useful for theoretical analyses, reference levels for the incident EMF are more commonly used for practical exposure assessments (ICNIRP 1998, IEEE 2005). These reference levels have been derived from the SAR limits through simulations modeling the human anatomy as prolate spheroid bodies (Gandhi 1980) or homogeneous blocks (Durney 1980). As individual anatomy is highly diverse, it is difficult to generalize the results from these simplistic models to the entire human population. Therefore, various anatomical models have been used in several studies to investigate the SAR_{wb} for plane wave exposure at the reference levels (Hirata *et al* 2007, 2009, Conil *et al* 2008, Nagaoka *et al* 2008, Wang *et al* 2006, Findlay and Dimbylow 2005, Dimbylow 2002, 2005, Sandrini *et al* 2004). These previous studies also examined the exposure of children by using approximated models, leading to simulation inaccuracies. According to the World Health Organization (WHO), correct anatomical models of children have been insufficiently examined, and further research is required to fill the gap in numerical modeling of children exposure assessments (WHO 2006).

Most of the previous studies use child models that are derived from down-scaling adult models, through either homothetic transformations or piecewise reductions (Conil *et al* 2008). However, due to anatomical changes that occur during adolescence, this scaling leads to inaccuracies, particularly in the skin thickness and proportions of the head and brain (Conil *et al* 2008). For tissue interfaces with high dielectric contrast, this might influence the accuracy of the SAR_{wb} and SAR_{10g} predictions (Christ and Kuster 2005). Only a limited number of studies have used anatomically correct models. Dimbylow and Bolch (2007) calculated the SAR_{wb} in five child models in the range of 9 months–14 years, and Kuhn *et al* (2009) used child models of 6 and 11 years old. Although the SAR_{wb} results are in good agreement with the down-scaled models, large differences were found for the SAR_{10g}. Hence, an extended evaluation using a sufficient set of anatomies is necessary to determine the exposure envelope for the entire population (Kuhn *et al* 2009).

Typically, peaks in both the SAR_{wb} and SAR_{10g} are present in two distinguishable frequency regions. The 'primary' peak $f_{res,peak1}$ in the 50–150 MHz region is related to the physical phenomenon of whole-body resonances occurring when the electric field is parallel to the main body axis. The 'secondary' peak f_{peak2} in the GHz band is related to the definition of the frequency-dependent ICNIRP reference levels (table 1).

Most of the current literature has studied frontal vertically aligned plane waves, as it was expected that the SAR_{wb} is maximum at this polarization at $f_{res,peak1}$.

Recent studies, including both scaled and anatomically correct models, have shown that SAR_{wb} can also peak at f_{peak2} for other incidences and polarizations (Dimbylow *et al* 2010, Uusitupa *et al* 2010, Hirata *et al* 2009, Kuhn *et al* 2009, Nagaoka *et al* 2008). The peaks of the SAR_{wb} at $f_{res,peak1}$ and at f_{peak2} are highly dependent on body size and anatomical structures. Therefore, the existing data should be rigorously verified at all incidences and polarizations, as well as for a variety of anatomically correct child models.

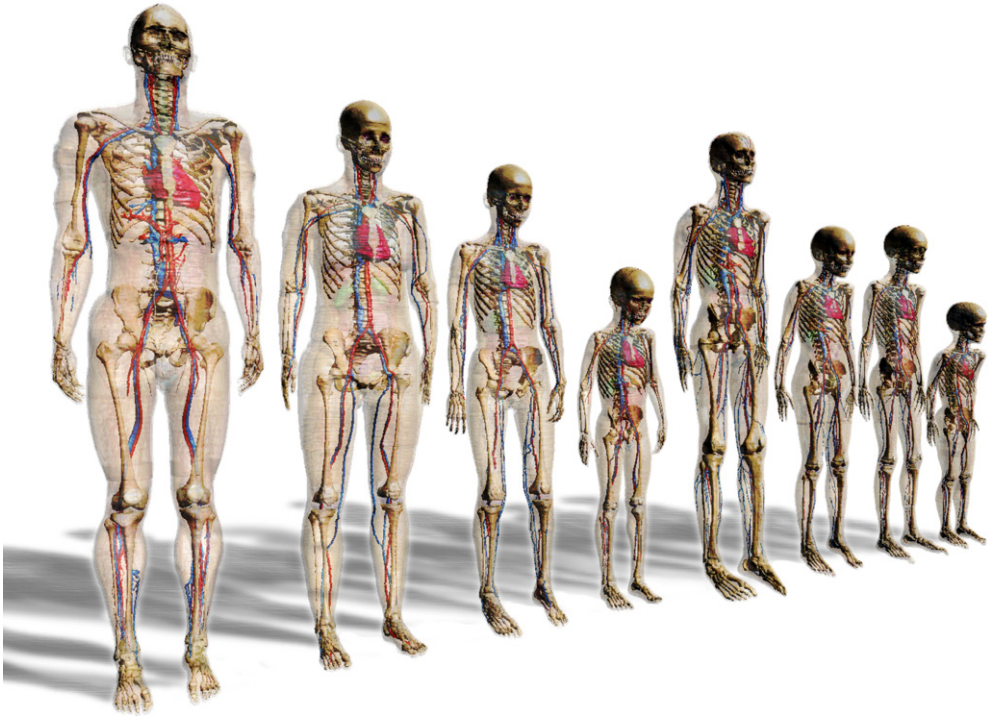

Figure 1. Virtual family models. From left to right: Duke, Ella, Billie, Thelonious, Louis, Eartha, Dizzy and Roberta.

The objective of this study was to assess if the induced SAR in children remains below the ICNIRP basic SAR restrictions for incident EMF exposure at the reference levels. In a brute-force approach, we assessed the induced SAR in anatomically correct models of six children by using 12 plane wave configurations, i.e. all orthogonal incidences and polarizations, and frequencies in the range of 10 MHz–5.6 GHz. For comparison, we also assessed the exposure for two adult models. Additional simulations with altered settings were used to asses the expanded uncertainty of the numerical results. SAR distributions of configurations, according to which the recommended reference levels are not consistent with the SAR restrictions, have been analyzed to understand the mechanisms regarding the spatial peak locations. Finally, we verified the consistency of our results by comparing them to the previously published exposure data.

2. Methods

First, we assessed the SAR_{wb} and peak 10 g spatial-averaged SAR (SAR_{10g}) in six child and two adult models. Second, we analyzed the SAR distributions and SAR_{10g} locations for configurations where SAR restrictions are exceeded. Third, we assessed the uncertainty and finally compared the results to the existing exposure data.

2.1. Human models

Figure 1 shows the eight models used in our dosimetric simulations. The models have been developed from high-resolution MRI data (Christ *et al* 2010) and are known as the 'virtual

Table 2. Characteristics of the anatomical models, ordered according to the line-up in figure 1. BMI is the body mass index.

Name	Sex	Age (years)	Height (m)	Weight (kg)	BMI (kg m^{-2})
Duke	Male	34	1.74	70	23.1
Ella	Female	26	1.60	58	22.7
Billie	Female	11	1.48	34	15.5
Thelonious	Male	6	1.17	17	12.4
Louis	Male	14	1.65	50	18.4
Eartha	Female	8	1.34	29	16.2
Dizzy	Male	8	1.36	25	13.5
Roberta	Female	5	1.09	16	13.5

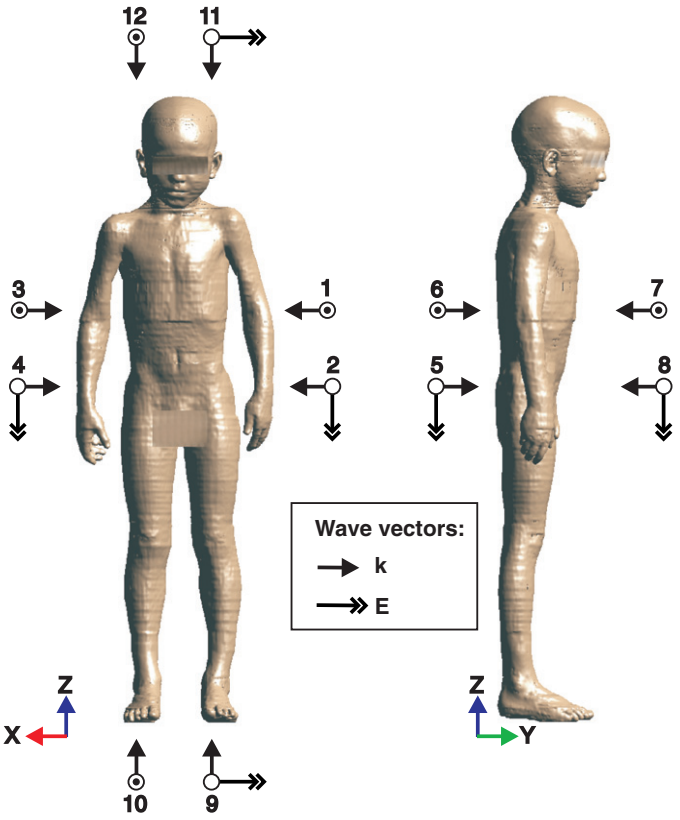

Figure 2. Visualization of the 12 orthogonal plane wave exposure configurations.

family' and 'virtual classroom'. They consist of six child and two adult models from both genders and with different body dimensions (table 2). The method of selecting tissue properties used in the models is explained in section 2.4.4.

2.2. Plane wave configurations

Plane waves were used with incident directions of the six major sides, i.e. frontal, dorsal, left, right, bottom and top (figure 2). In addition, we used two orthogonal polarizations

Table 3. Number of grid-steps in tissues, Δ_{tissue}, per wavelength at the tissue with maximum relative dielectric permittivity $\lambda_{\epsilon_{r,\max}}$. Note that we used $\Delta_{\text{tissue}} = 2$ mm for $f < 2400$ and $\Delta_{\text{tissue}} = 1$ mm for $f \geqslant 2400$ MHz.

f (MHz)	$\epsilon_{r,\max}$	$\text{tissue}_{\epsilon_{r,\max}}$	$\lambda_{\epsilon_{r,\max}}/\Delta_{\text{tissue}}$
10	488	Small intestine	680
100	98	Kidney cortex	150
1000	70	Gallbladder	18
1800	69	Gallbladder	10
2400	69	Gallbladder	15
3200	68	Eye vitreous humor	11
5600	65	Eye vitreous humor	**6**

of the electric field per incident direction. We used frequencies in the range of 10 MHz–5.6 GHz, with specific refinements at $f_{\text{res,peak1}}$ and f_{peak2} to find the peak values. The frequency-dependent ICNIRP reference levels for the general public (table 1) were used for the plane wave power density S_{eq}, to enable evaluation if the basic SAR restrictions are exceeded. Including additional simulations for assessing the numerical uncertainty, the 12 plane wave configurations at 20 frequencies and eight human models resulted in more than 2200 scenarios.

2.3. Numerical model

SEMCAD X (Speag, Switzerland) was used for the modeling, simulation and analysis of the plane wave configurations. Its finite difference time domain (FDTD) solver was used to numerically evaluate the electromagnetic wave propagation and interaction with the body (Taflove and Hagness 2005). A rectangular Huygens surface with electromagnetic sources (Merewether *et al* 1980) was used to produce the correct total field inside and the scattered field outside the surface, also known as the total-field scattered-field (TFSF) technique. A minimum separation of five mesh cells between the human models and the Huygens surface was used to avoid intersection and to describe the plane waves accurately.

Uni-axial perfectly matched layers (UPML), at a 20 mm distance from the Huygens surface, were applied to avoid reflections back into the computational domain. A UPML efficiency of $\geqslant$95% was used to automatically generate the layers and its absorbing profile, based on modified geometrical progressions (SPEAG 2009). As a result, the number of UPML was in the range of 7 at 5.6 GHz to 14 at 10 MHz.

To ensure steady-state EMF , the number of harmonic periods corresponds to a propagation distance of at least two times the maximum diameter of the computational domain. Another restriction is a minimum of two periods since we used one period to ramp the envelope of the sinusoidal excitation waveform. This ramp function was used to minimize the generation of other frequency components outside the main carrier at the start of the pulse train.

To obtain adequate sampling, the maximum grid-step in tissues, Δ_{tissue}, allowed is $\lambda_{\text{tissue}}/10$, based on tissues with the maximum dielectric permittivity ($\epsilon_{r,\max}$) (table 3). Outside the body, the grid step was gradually increased by a factor 1.3 to maximum $\lambda/15$ in free space.

2.3.1. SAR_{wb} and $SAR_{10\text{g}}$. The SAR in a single FDTD cell and the localized peak SAR are calculated based on annex E of IEEE C95.3 (IEEE 2002). To compute the SAR for a single FDTD cell, the complex vector components of the electric field at each individual cell edge are averaged into the voxel center using linear interpolation (Caputa *et al* 1999). The absorption

rate in all cells is summed and then divided by the mass of the whole body, to obtain the SAR_{wb}.

A special 'fast' strategy is used to find the overall maximum of the peak localized SAR, averaged over a 10 g cube (SAR_{10g}), as required in the current IEEE guidelines. Although this strategy does not calculate the peak SAR at full resolution in the regions with lower absorption, the overall maximum is identical to the peak SAR defined in the IEEE standard.

2.4. Numerical uncertainty

To investigate the overall uncertainty (ISO/IEC 2008, Taylor and Kuyatt 1994) of the numerical modeling, we determined the influence of various modeling parameters on the obtained results, i.e. SAR_{wb} and SAR_{10g}. The investigated modeling parameters were (1) model discretization, (2) absorbing boundary conditions, (3) deviations from steady state, (4) plane wave homogeneity and (5) tissue properties.

2.4.1. Model discretization. The effect of the spatial resolution in the model discretization was investigated by simulating the grid steps (Δ) between 0.7 mm and 10 mm for the Thelonious model. Although both SAR_{wb} and SAR_{10g} converge for decreasing Δ, the rate of convergence depends on frequency, wave incidence and polarization. Therefore, we evaluated this convergence for all 12 plane wave configurations and for the frequencies 10, 100, 1000, 1800, 3200 and 5600 MHz. To estimate the converged value for $\Delta \rightarrow 0$, we fitted a quadratic curve to the data in the range of 0.7–3 mm. The analysis was simplified by using the maximum error of the 12 plane wave configurations. We used $\Delta = 2$ for $f < 2000$ and $\Delta = 1$ mm for $f \geqslant 2000$ MHz since we allowed a maximum SAR_{wb} error of $\pm 5\%$ due to the discretization.

The effect of using a uniform expanding grid step was investigated by using additional simulations with a uniform spaced grid. For this analysis, we assumed that the induced dispersion error becomes maximum for the smallest grid step, i.e. 1 mm and for the maximum frequency, i.e. 5.6 GHz.

2.4.2. Absorbing boundary conditions and deviations from steady state. We estimated the uncertainty contribution of deviation from steady-state fields and imperfect ABCs simultaneously. We increased the efficiency of the UMPL by using additional absorbing layers. In addition, we increased the distance from the Huygens surface to the ABCs from 20 mm to $\lambda_{\mathbf{air}}/2$. Also additional time steps were used to increase the number of periods of the harmonic wave in order to propagate at least two times through the computational domain, applying a maximum ϵ_r of tissue instead of air, to calculate the wave speed. As a result, the number of periods was increased from 2 to 2.5 at 10 MHz and from 20 to 170 at 1800 MHz.

Since these uncertainties depend on the frequency, incidence, polarization and human model, we investigated the uncertainty for both 10 MHz and 1.8 GHz, two incidences and polarizations (cases 8 and 12) to all models. Due to limitations in memory resources of our simulation hardware, we were not able to estimate the ABCs and steady-state uncertainty for $f \geqslant 1800$ MHz. We simplified the analysis by using the maximum error of both frequencies and both plane wave configurations.

2.4.3. Plane wave homogeneity. The incident plane waves were excited by a rectangular Huygens surface (Merewether *et al* 1980) and the maximum error in the electric field amplitude was obtained for the smallest λ/Δ at 5.6 GHz. By using field sensors, we determined the maximum deviation in the homogeneous wave front. Since the SAR was quadratically related to E, the uncertainty in the SAR was doubled.

2.4.4. Tissue properties. A 4-Cole–Cole dispersion model for each tissue type was used to assign the frequency-dependent relative permittivity (ϵ_r) and effective conductivity (σ), according to the commonly used literature review Gabriel *et al* (1996a), (1996b), (1996c). For the 'mass' specific-absorption-rate (SAR), we assigned the volume density of mass (ρ) according to the mean literature values of Duck (Cameron 1991). For individuals however, the tissue properties deviate from the mean literature values, which influences the values for the SAR_{wb} and SAR_{10g}.

Volume density of mass. There is a variation in the measured ρ of $\pm 10\%$ in most of the tissues, while up to $\pm 50\%$ is reported for the lungs (McIntosh and Anderson 2009). These variations directly affects the SAR values; however, we excluded the variation in the lungs since we assume that the influence on the SAR_{wb} and SAR_{10g} are negligible due to the low fields at this location.

Permittivity and conductivity. There is a maximum 90% age-dependent decline in the dielectric properties of tissues with low water content, such as fat and bone (Peyman *et al* 2009, Gabriel 2005). The influence of this decline on the SAR_{wb} and SAR_{10g} was investigated by applying the changes to the Thelonious model for the exposure configuration 8 at 900 and 1800 MHz (Christ *et al* 2009).

Additionally, assumptions were made to assign literature values to tissues where either no data or multiple data were available. For example, we use dry and not wet skin and fat that is average infiltrated instead of not infiltrated by blood. The influence of these choices on the SAR_{wb} and SAR_{10g} for the exposure configuration 8 at $f = 1800$ MHz is 10.7% (Dimbylow *et al* 2008). For other configurations and frequencies, the influence is unknown.

Further, the 4-Cole–Cole parameters provide only a 'best estimate', due to measurement uncertainties and variations in the literature (Gabriel and Peyman 2006). Although the influence of these dielectric changes on SAR_{wb} and SAR_{10g} is unknown, we do know that the variations are much smaller than the age-dependent dielectric changes. Therefore, we estimated the influence of dielectric measurement uncertainties on the SAR_{wb} and SAR_{10g} by a 25% fraction of the influence caused by age-dependent dielectric changes.

Finally, the dielectric properties are mostly obtained from excised tissue, while post-mortal changes up to 18% occur immediately after death, as a consequence of stopped circulation (Burdette *et al* 1986, Schmid *et al* 2003, Schmid and Uberbacher 2005). Although the influence on the SAR_{wb} and SAR_{10g} is unknown, these changes are much smaller than the age-dependent changes, and therefore we use a 25% fraction of the age-dependent result.

3. Results

We first analyzed the SAR_{wb} and SAR_{10g} data for the eight human models exposed to the 12 plane wave configurations. The worst-case summary for models is shown in figure 4. We then focused on the SAR distributions where ICNIRP basic restrictions were exceeded. Finally, we provided an example to demonstrate the typical SAR_{10g} locations for the Thelonious model.

3.1. Comparison of the calculated SAR to basic restrictions

Figure 3 shows the SAR_{wb} and SAR_{10g} for all frequencies and exposure configurations in the Thelonious model. We visualize this only since we observed similar trends for the other

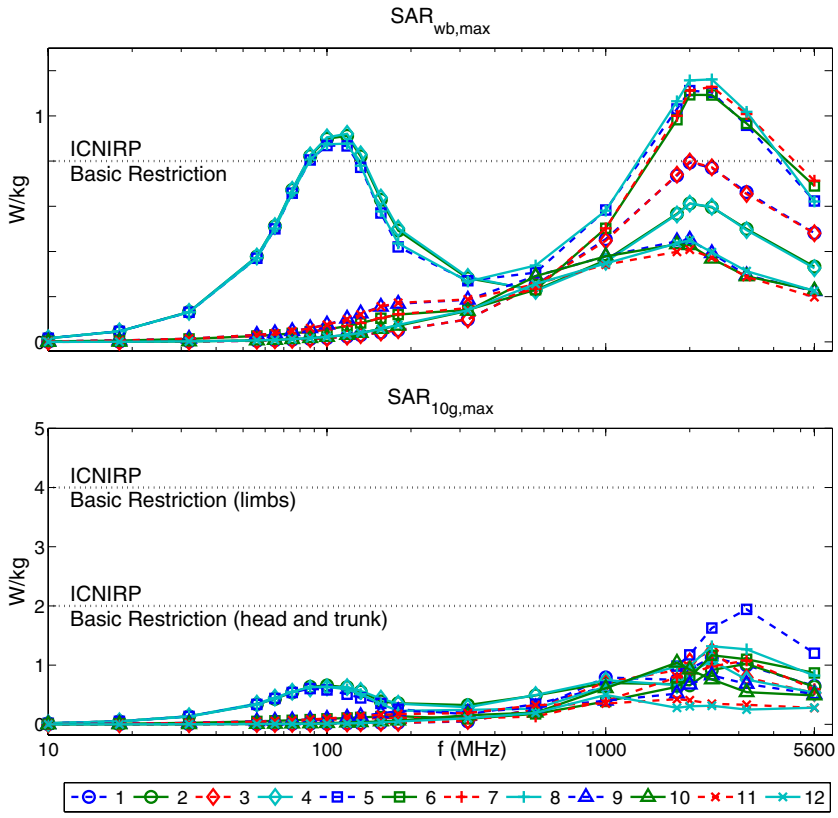

Figure 3. SAR_{wb} (top) and SAR_{10g} (bottom) for exposure at the ICNIRP reference level in the Thelonious model for 12 plane wave configurations.

models. Figure 4 shows the worst-case maximum exposure scenarios, highlighting the model and frequency combinations where exposure at ICNIRP reference levels leads to exposure above the basic restrictions.

These figures confirm that the SAR_{10g} is increased at two frequency bands, i.e. at $f_{res,peak1}$ and at f_{peak2}. Figure 4 shows the over-exposure of the SAR_{wb} at $f_{res,peak1}$ for the small models, i.e. Billie, Thelonious, Eartha, Dizzy and Roberta. A closer analysis reveals that this occurs only for configurations with the electric field aligned parallel to the main body axis, i.e. configurations 2, 4, 5 and 8. Note that the ratio between the body height and wavelength in air at $f_{res,peak1}$ is 0.4 ± 0.02 for all models.

At f_{peak2}, the SAR_{wb} over-exposure of max 45% occurs also for the same small models for the configuration with maximum body surface illumination, i.e. configurations 5, 6, 7 and 8.

For the SAR_{10g} the same tendencies were observed as for the SAR_{wb}. Note that for some frequencies, the SAR_{10g} limits for head and trunk were exceeded. Closer analysis revealed that this high SAR_{10g} was confined to the limbs, for which a higher limit is defined. Hence, the SAR_{10g} is within the limits for all cases.

Numerical uncertainty. To determine the expanded uncertainty U of the numerical modeling with 95% confidence, we assessed the influence of various modeling parameters on the simulation results. Table 4 shows that U is 53% for the SAR_{wb} and 58% for the SAR_{10g}.

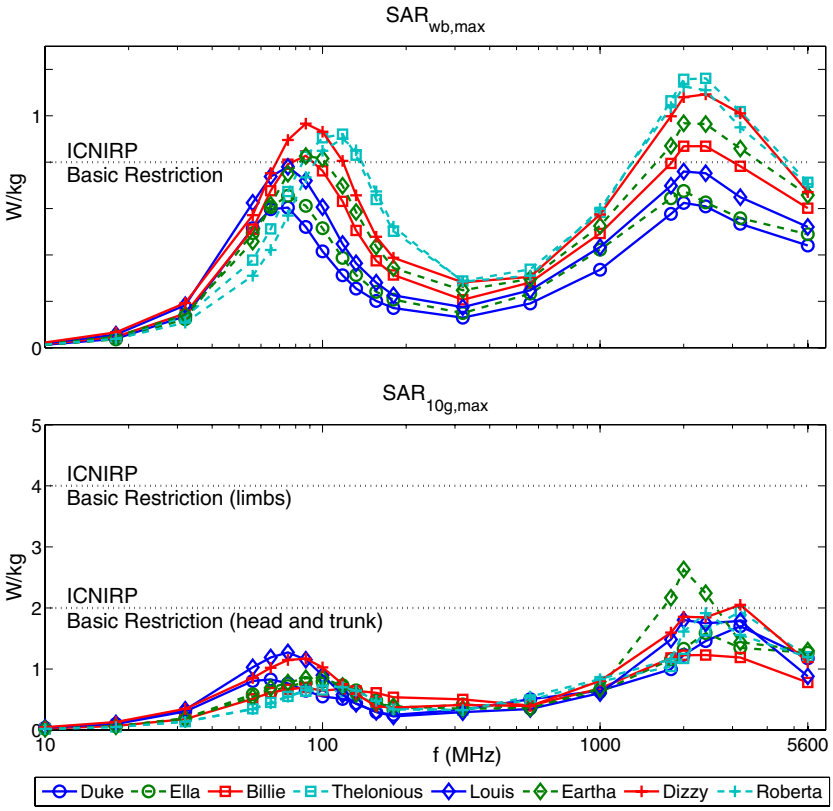

Figure 4. Worst case SAR_{wb} (top) and SAR_{10g} (bottom) in the eight human models for 12 plane wave configurations. Note that the locations where the SAR_{10g} restrictions for head and trunk are exceeded are all located in the limbs.

3.2. Closer analysis of SAR distributions at configurations which exceed the basic restrictions

To assess thermal relevance, we analyzed the SAR distributions and peak locations for configurations that exceeded the basic restrictions. In addition, we also examined typical peak SAR_{10g} locations.

3.2.1. Example SAR distributions in Thelonious at $f_{res,peak1}$ and f_{peak2}. Figure 5 demonstrates, for the exposure configuration 8, the SAR distributions at the frequencies where the basic restrictions were exceeded, i.e. at $f_{res,peak1}$ (a,b) and at f_{peak2} (c,d). Note that the color scaling is very sensitive to peak values since spatial averaging is not used.

At $f_{res,peak1}$, high SAR values are shown at the ankles, knees and the neck and at both superficial and deep locations.

At $f_{res,peak2}$, the illuminated sides of the model show high SAR values, while the 'shadow' sides have a low SAR. Although not shown here, this also applies for the other exposure configurations and models. Peak SAR values are observed at body protrusions such as the nose, chin, fingers and toes.

Figure 6 shows that similar distributions are obtained at $f_{res,peak1}$ for the other exposure configurations where the basic restrictions are exceeded, i.e. configurations 2, 4 and 5.

Table 4. Evaluation of the standard combined uncertainty u_c and the expanded uncertainty U of the whole-body (wb) or spatial averaged over 10 g tissue (10 g) SAR. Div. is the division factor to obtain the standard uncertainty (std. unc.) and k is the coverage factor. The sensitivity coefficients c_i equals one for all uncertainty contributions.

	SAR unc. %				SAR std. unc. %	
	wb	10 g	Prob. distr.	Div.	wb	10 g
Discretization						
(a) spatial resolution	5.0	11.9	Normal	2	2.5	5.5
(b) non-uniform grid	1	1	Normal	2	0.5	0.5
ABC + steady-state dev.	6.0	3.5	Rect.	$\sqrt{3}$	3.5	2.0
Wave homogeneity	1.0	1.0	Normal	1	1.0	1.0
ρ	10.0	10.0	Normal	2	5.0	5.0
ϵ_r, σ						
(a) Age-dependence	5.8	6.5	Normal	1	5.8	6.5
(b) Tissue assignment	10.7	10.7	Normal	2	5.4	5.4
(c) 4-Cole–Cole	1.5	1.6	Normal	1	1.5	1.6
(d) Post-mortal changes	1.5	1.6	Normal	1	1.5	1.6
u_c ($k = 1$)					27	29
U ($k = 2$)					53	58

At f_{peak2}, the 'shadowing' effect due to low penetration is also shown for the other peak configurations, i.e. 5, 6 and 7. Although not shown here, this applies also for the other exposure configurations and models.

Peak SAR_{10g} locations are mostly at the body protrusions such as the nose, chin, fingers, toes, shoulders, armpits, wrests, ankles, male organ and the tail bone. For the frequencies below 1000 MHz, these peak locations are 'grouped' by the field polarization. Although not shown here, these typical locations and polarization dependence are also present at other frequencies and in other models.

4. Discussion

In this study, we investigated the SAR_{wb} and SAR_{10g} in anatomical models of six children and two adults when exposed to all orthogonal plane wave configurations at frequencies in the range of 10 MHz–5.6 GHz. In this study, we found that for worst-case exposure scenarios, the ICNIRP basic restrictions on the SAR_{wb} are exceeded for small children by maximum 45%, which is in agreement with the existing data that used both scaled and anatomically correct models. The result of the expanded uncertainty analysis (54% for $k = 2$) revealed that the over-exposure is limited to 120% for these generic plane wave scenarios.

Evaluation of the methods. In our opinion, a rigorous uncertainty assessment should be included when testing the consistency of the ICNIRP reference levels. Although various studies have tested the validity of their code and the influence of various modeling parameters on the results, a complete uncertainty evaluation is usually not included. The validity of the FDTD implementations is usually tested by comparison to an analytical Mie series solution for a homogeneous sphere (Neuder 1979). The influence of the distance from the human model to the absorbing boundaries is investigated in e.g. Findlay and Dimbylow (2006) and

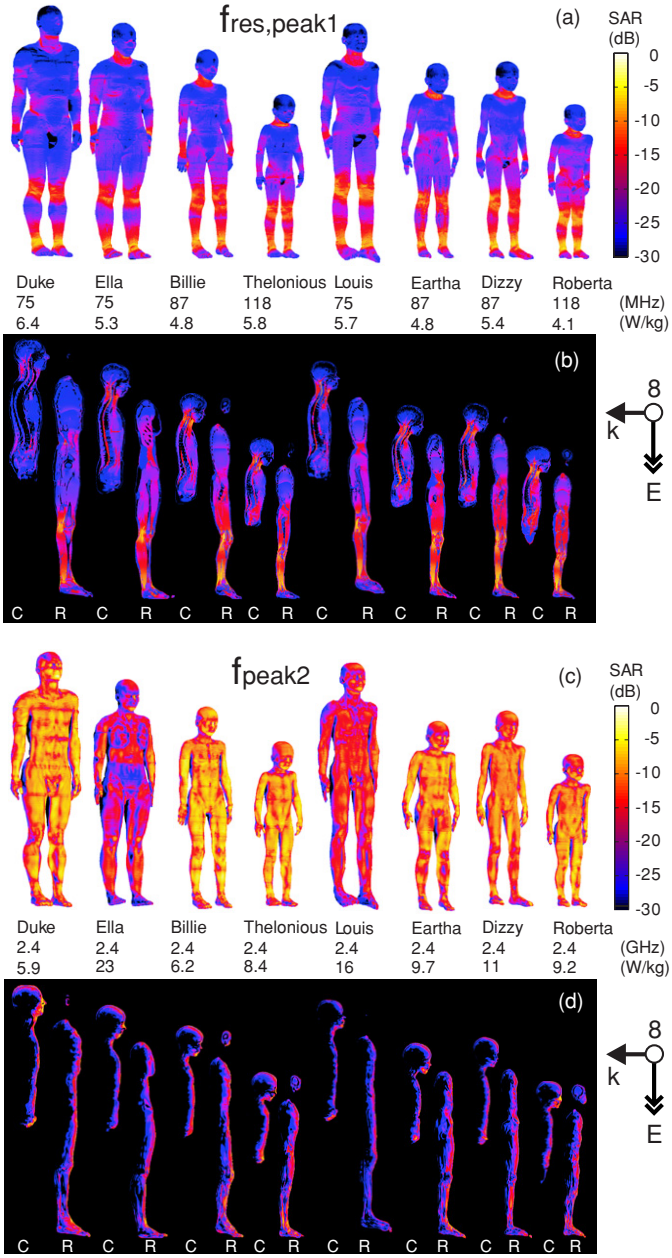

Figure 5. Surface SAR and SAR in slices through the central body axis (C) and right leg (R) in all models at $f_{\mathrm{res,peak1}}$ (a,b) and at f_{peak2} (c,d) for the plane wave configuration 8. The SAR values indicate the maximum SAR in the model.

the influence of discretization and deviation from steady-state signals in Kuhn *et al* (2009). Fortunately, recent advances (Peyman *et al* 2009, Gabriel 2005) made it possible to estimate the influence of age-dependent tissues. In addition, we assessed the uncertainty of volume mass density and variation in dielectric properties due to tissue assignment, 4-Cole–Cole

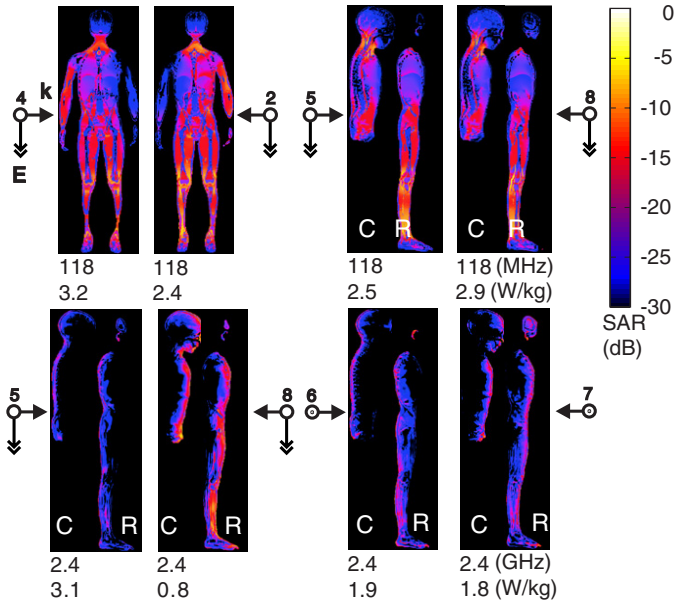

Figure 6. SAR in slices through the central body axis (C) and right leg (R) of Thelonious exposed to the worst-case plane wave configurations at $f_{\mathrm{res,peak1}}$ (top) and at f_{peak2} (bottom).

dispersion model and post-mortal changes. Although we provided an extensive uncertainty analysis with our results, it is recommended to further investigate the influence on the $\mathrm{SAR_{wb}}$ and $\mathrm{SAR_{10g}}$ for more plane wave configurations. Standardized techniques are required for the validation of an FDTD code and for the assessment of the uncertainty of numerical results.

In this study, we compared the peak localized SAR averaged over a 10 g cube ($\mathrm{SAR_{10g}}$) with the ICNIRP guidelines. However, contiguous region averaging is required in these guidelines, and therefore a direct comparison to the ICNIRP guidelines of 2 W $\mathrm{kg^{-1}}$ (head and trunk) and 4 W $\mathrm{kg^{-1}}$ (limbs) cannot be made. Contiguous averaging is more conservative (up to a factor of 2.5) than averaging over a cube (Findlay and Dimbylow 2008). Our results are consistent when comparing to IEEE guidelines (IEEE 2005) which prescribes 10 g cube averaging to restrict the localized SAR to 2 W $\mathrm{kg^{-1}}$ (localized) and 4 W $\mathrm{kg^{-1}}$ (extremities and pinnae). However, for contiguous averaging, the $\mathrm{SAR_{10g}}$ might exceed the ICNIRP basic restriction on the localized SAR in the head and trunk.

In this study, the human models were exposed to plane waves under free-space conditions. The introduction of a ground plane leads to several differences, i.e. scattering effects and body resonance changes. When an EMF is normal or oblique incident to a ground plane, the combination of the original plane wave and its reflection causes an inhomogeneous exposure in the vertical direction. However, when normalizing the total exposure to the spatially averaged field, the locally increased field values do not induce higher exposures with respect to the free-space plane wave (Findlay and Dimbylow 2008, Kuhn *et al* 2009). For frontal and vertically aligned electric fields, i.e. configuration 8, the ground plane causes the body's resonant frequency $f_{\mathrm{res,peak1}}$ to shift approximately to $f_{\mathrm{res,peak1}}/2$, but no increase in exposure (Dimbylow 2005, 1997).

It was recommended (Kuhn *et al* 2009) to extend the frequencies below 50 MHz and above 2.45 GHz to determine the exposure envelope. Our results demonstrate that the SAR

values are not increased for frequencies below 50 MHz. The envelope of the second peak extends to 4 GHz for the small children, i.e. Thelonious, Roberta and Dizzy. These findings are in agreement with the existing data (Dimbylow *et al* 2010, Uusitupa *et al* 2010, Findlay *et al* 2009, Hirata *et al* 2009, Conil *et al* 2008, Dimbylow and Bolch 2007).

Evaluation of the results. The ICNIRP reference levels for the high-frequency incident EMF have been derived by using simulations with humans modeled as a prolate spheroid body (Gandhi 1980, ICNIRP 1998). In this derivation, a SAR_{wb} of 4 W kg^{-1} induces a body temperature increase of less than 1 °C. A safety factor of 50 is applied to the basic SAR restriction to avoid excessive heating for the general public. Additional factors are used also in the reference levels to account for 'differences in absorption by individuals of different sizes and different orientations relative to the field'. Despite these additional factors, we have demonstrated that for children smaller than 1.48 m, the basic SAR_{wb} restrictions of 0.08 W kg^{-1} are exceeded at the EMF reference levels. Note that we used standing models, while the SAR values can be averaged over 6 min, and it is unlikely that small children can stand straight for this length of time.

Previous studies have applied mainly frontal vertically aligned plane waves, i.e. configuration 8, since the SAR_{wb} is maximum for this configuration at $f_{res,peak1}$. Analysis of our results revealed that the SAR_{wb} is maximum also for other incidences with similar polarizations, i.e. configurations 2, 4 and 5. At $f_{res,peak1}$, the basic restrictions on the SAR_{wb} are exceeded by maximum 20% (Dizzy), 15% (Thelonious and Roberta) and 10% (Billie, Louis and Eartha). These findings are consistent (5%) with the existing data obtained using the Thelonious model (Kuhn *et al* 2009). Note that deviations might be caused by a small difference in $f_{res,peak1}$.

At f_{peak2}, the SAR_{wb} is maximum for configurations with maximum body surface illumination, i.e. configurations 5, 6, 7 and 8. The basic restrictions on the SAR_{wb} are exceeded by maximum 45% (Thelonious), 41% (Roberta), 37% (Dizzy), 21% (Eartha) and 9% (Billie). The restrictions are not exceeded for the taller models, i.e. Duke, Ella and Louis. These findings are consistent (10%) with the existing data obtained using the Thelonious model (Uusitupa *et al* 2010, Kuhn *et al* 2009).

Figure 7 demonstrates that our SAR_{wb} results of configuration 8 are in good agreement with the previously published data, which includes both scaled and anatomically correct models (Uusitupa *et al* 2010, Dimbylow 1997, 2002, Dimbylow *et al* 2008, 2010, Kuhn *et al* 2009, Findlay *et al* 2009, Conil *et al* 2008, Nagaoka *et al* 2008, Dimbylow and Bolch 2007). Note that we sorted the results by body mass index (BMI) to distinct between the models. Differences in the results are explained by the various human models. Further confounding factors are uncertainties of the simulations and small differences in frequency because not all authors provide data from simulations precisely at $f_{res,peak1}$ and f_{peak2}.

Typical locations of the SAR_{10g} peaks are found at body protrusions, which is in agreement with the previously published data (Kuhn *et al* 2009). The exact location and value is strongly dependent on the model geometry; hence, it is highly sensitive to the segmentation of the tissues and it is favorable to use realistic rather than scaled anatomies. We found that the probability of the peak locations is related to the polarization of the electric field rather than to the incidence direction, which might be clarified by partial body resonances. In this study, we used orthogonal field polarizations, which are a good approach to asses the worst-case SAR_{wb} (Uusitupa *et al* 2010). However, this publication further shows that for the SAR_{10g}, the maximum values can also be obtained for oblique incidences and polarizations.

For all anatomical models, we observed that $f_{res,peak1}$ is related to the body height by a factor of 0.4, which is also found by Dimbylow *et al* (2008). Our results also show a secondary

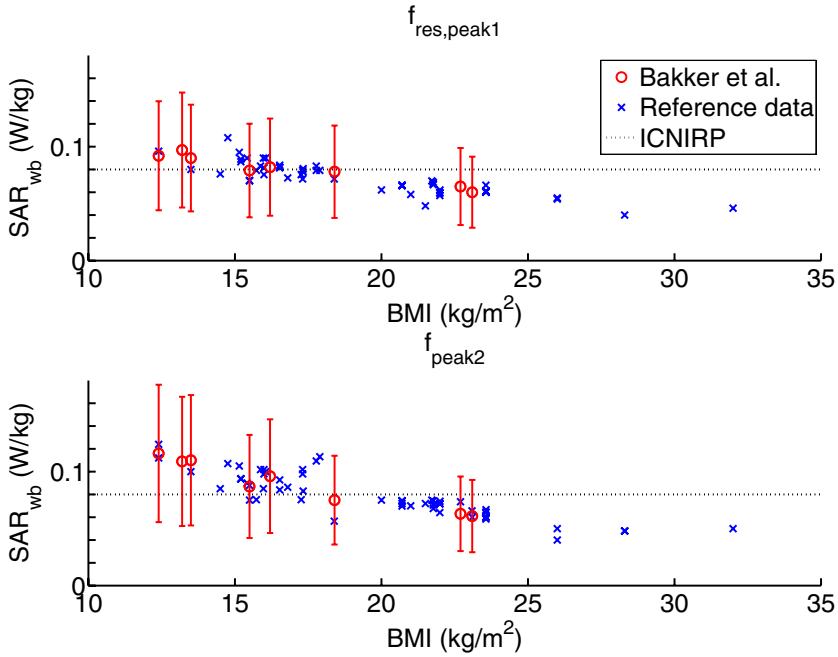

Figure 7. Comparison with reference data of the SAR_{wb} at $f_{res,peak1}$ (top) and f_{peak2} (bottom) for the plane wave configuration 8. The error bars indicate the expanded uncertainty U with a coverage factor $k = 2$.

peak at f_{peak2}, for plane waves incident to the front or back, since it corresponds to the largest illuminated cross-section.

5. Conclusions

In this study, we investigated the SAR_{wb} and SAR_{10g} in anatomical models of six children and two adults that are exposed to 12 orthogonal plane wave configurations at the ICNIRP reference levels for the EMF. The ICNIRP basic restrictions on the SAR_{wb} are exceeded for small children by maximum 45%. We do note that this is a very minor over-exposure when compared to the safety factor of 50.

Acknowledgments

This study was supported by The Netherlands Organization for Health Research and Development ZonMw.

References

Burdette E, Friederich P, Seaman R and Larsen L 1986 *In situ* permittivity of canine brain: regional variations and postmortem changes *IEEE Trans. Microw. Theory Tech.* **34** 38–50

Cameron J 1991 Physical Properties of Tissue. A Comprehensive Reference Book, edited by Francis A Duck *Med. Phys.* **18** 834

Caputa K, Okoniewski M and Stuchly M 1999 An algorithm for computations of the power deposition in human tissue *IEEE Antennas Propag. Mag.* **41** 102–7

Christ A *et al* 2010 The virtual family-development of surface-based anatomical models of two adults and two children for dosimetric simulations *Phys. Med. Biol.* **55** N23–38

Christ A and Kuster N 2005 Differences in RF energy absorption in the heads of adults and children *Bioelectromagnetics* **26** (Suppl. 7) S31–44

Christ A, Schmid G, Djafarzadeh R, Überbacher R, Cecil S, Zefferer M, Neufeld E, Lichtsteiner M, Bouterfas M and Kuster N 2009 Numerische bestimmung der spezifischen absorptionsrate bei ganzkörperexposition von kindern: Abschlußbericht, techreport, IT'IS Foundation, ETH Zurich, Zeughausstrasse 43, 8004 Zurich, Switzerland

Conil E, Hadjem A, Lacroux F, Wong M F and Wiart J 2008 Variability analysis of SAR from 20 MHz to 2.4 GHz for different adult and child models using finite-difference time-domain *Phys. Med. Biol.* **53** 1511–25

Dimbylow P 2005 Resonance behaviour of whole-body averaged specific energy absorption rate (SAR) in the female voxel model, NAOMI *Phys. Med. Biol.* **50** 4053–63

Dimbylow P and Bolch W 2007 Whole-body-averaged SAR from 50 MHz to 4 GHz in the University of Florida child voxel phantoms *Phys. Med. Biol.* **52** 6639–49

Dimbylow P, Bolch W and Lee C 2010 SAR calculations from 20 MHz to 6 GHz in the University of Florida newborn voxel phantom and their implications for dosimetry *Phys. Med. Biol.* **55** 1519–30

Dimbylow P J 1997 FDTD calculations of the whole-body averaged SAR in an anatomically realistic voxel model of the human body from 1 MHz to 1 GHz *Phys. Med. Biol.* **42** 479–90

Dimbylow P J 2002 Fine resolution calculations of SAR in the human body for frequencies up to 3 GHz *Phys. Med. Biol.* **47** 2835–46

Dimbylow P J, Hirata A and Nagaoka T 2008 Intercomparison of whole-body averaged SAR in European and Japanese voxel phantoms *Phys. Med. Biol.* **53** 5883–97

Durney C 1980 Electromagnetic dosimetry for models of humans and animals: a review of theoretical and numerical techniques *Proc. IEEE* **68** 33–40

Findlay R P and Dimbylow P J 2005 Effects of posture on FDTD calculations of specific absorption rate in a voxel model of the human body *Phys. Med. Biol.* **50** 3825–35

Findlay R P and Dimbylow P J 2006 Variations in calculated SAR with distance to the perfectly matched layer boundary for a human voxel model *Phys. Med. Biol.* **51** N411–5

Findlay R P and Dimbylow P J 2008 Calculated SAR distributions in a human voxel phantom due to the reflection of electromagnetic fields from a ground plane between 65 MHz and 2 GHz *Phys. Med. Biol.* **53** 2277–89

Findlay R P, Lee A K and Dimbylow P J 2009 FDTD calculations of SAR for child voxel models in different postures between 10 MHz and 3 GHz *Radiat. Prot. Dosim.* **135** 226–31

Gabriel C 2005 Dielectric properties of biological tissue: variation with age *Bioelectromagnetics* **26** (Suppl. 7) S12–8

Gabriel C, Gabriel S and Corthout E 1996a The dielectric properties of biological tissues: I. Literature survey *Phys. Med. Biol.* **41** 2231–49

Gabriel C and Peyman A 2006 Dielectric measurement: error analysis and assessment of uncertainty *Phys. Med. Biol.* **51** 6033–46

Gabriel S, Lau R W and Gabriel C 1996b The dielectric properties of biological tissues: II. Measurements in the frequency range 10 Hz to 20 GHz *Phys. Med. Biol.* **41** 2251–69

Gabriel S, Lau R W and Gabriel C 1996c The dielectric properties of biological tissues: III. Parametric models for the dielectric spectrum of tissues *Phys. Med. Biol.* **41** 2271–93

Gandhi O 1980 State of the knowledge for electromagnetic absorbed dose in man and animals *Proc. IEEE* **68** 24–32

Hirata A, Ito N and Fujiwara O 2009 Influence of electromagnetic polarization on the whole-body averaged SAR in children for plane-wave exposures *Phys. Med. Biol.* **54** 59–65

Hirata A, Kodera S, Wang J and Fujiwara O 2007 Dominant factors influencing whole-body average SAR due to far-field exposure in whole-body resonance frequency and GHz regions *Bioelectromagnetics* **28** 484–7

ICNIRP (International Commission on Non Ionizing Radiation Protection) 1998 Guidelines for limiting exposure to time-varying electric, magnetic, and electromagnetic fields (up to 300 GHz) *Health Phys.* **74** 494–522

IEEE 2002 Recommended practice for measurements and computations of radio frequency electromagnetic fields with respect to human exposure to such fields, 100 kHz–300 GHz *Std C95.3* (New York: IEEE)

IEEE 2005 Standard for safety levels with respect to human exposure to radio frequency electromagnetic fields, 3 kHz to 300 GHz *Std C95.1* (New York: IEEE)

ISO/IEC 2008 Uncertainty of measurement: part 3. Guide to the expression of uncertainty in measurement (GUM:1995) *ISO/IEC Guide 98-3: 2008/Suppl 1: 2008/Cor 1: 2009* http://www.iso.org/iso/catalogue_detail.htm?csnumber=54350

Kuhn S, Jennings W, Christ A and Kuster N 2009 Assessment of induced radio-frequency electromagnetic fields in various anatomical human body models *Phys. Med. Biol.* **54** 875–90

McIntosh R and Anderson V 2009 A comprehensive tissue properties database provided for the thermal assessment of a human at rest *BIOEM2009, Joint Meeting of the Bioelectromagnetics Society and the European BioElectromagnetics Association*

Merewether D E, Fisher R and Smith F W 1980 On implementing a numeric Huygen's source scheme in a finite difference program to illuminate scattering bodies *IEEE Trans. Nucl. Sci.* **27** 1829–33

Nagaoka T, Kunieda E and Watanabe S 2008 Proportion-corrected scaled voxel models for Japanese children and their application to the numerical dosimetry of specific absorption rate for frequencies from 30 MHz to 3 GHz *Phys. Med. Biol.* **53** 6695–711

Neuder S M 1979 Electromagnetic fields in biological media: part 2. The SCAT program, multilayered spheres, theory and applications *HEW Publication (FDA)* pp 79–8072

Peyman A, Gabriel C, Grant E H, Vermeeren G and Martens L 2009 Variation of the dielectric properties of tissues with age: the effect on the values of SAR in children when exposed to walkie-talkie devices *Phys. Med. Biol.* **54** 227–41

Sandrini L, Vaccari A, Malacarne C, Cristoforetti L and Pontalti R 2004 RF dosimetry: a comparison between power absorption of female and male numerical models from 0.1 to 4 GHz *Phys. Med. Biol.* **49** 5185–201

Schmid G, Neubauer G, Illievich U M and Alesch F 2003 Dielectric properties of porcine brain tissue in the transition from life to death at frequencies from 800 to 1900 MHz *Bioelectromagnetics* **24** 413–22

Schmid G and Uberbacher R 2005 Age dependence of dielectric properties of bovine brain and ocular tissues in the frequency range of 400 MHz to 18 GHz *Phys. Med. Biol.* **50** 4711–20

SPEAG 2009 *SEMCAD X Reference Manual* Schmid & Partner Engineering AG

Taflove A and Hagness S 2005 *Computational Electrodynamics: The Finite-Difference Time-Domain Method* 3rd edn (Norwood, MA: Artech House Publishers)

Taylor B and Kuyatt C 1994 Guidelines for evaluating and expressing the uncertainty of NIST measurement results *NIST Technical Note 1297*

Uusitupa T, Laakso I, Ilvonen S and Nikoskinen K 2010 SAR variation study from 300 to 5000 MHz for 15 voxel models including different postures *Phys. Med. Biol.* **55** 1157–76

Wang J, Fujiwara O, Kodera S and Watanabe S 2006 FDTD calculation of whole-body average SAR in adult and child models for frequencies from 30 MHz to 3 GHz *Phys. Med. Biol.* **51** 4119–27

WHO (World Health Organization) 1993 *Environmental Health Criteria 137—Electromagnetic Fields (300 Hz to 300 GHz)*

WHO (World Health Organization) 2006 *Research Agenda for Radio Frequency Fields*